CMS Physics Analysis Summary

Contact: cms-pag-conveners-higgs@cern.ch 2016/03/21

Search for $pp \to H \to ZA \to l^+l^-b\bar{b}$ with 2015 data

The CMS Collaboration

Abstract

This note details the search for a CP-even (H) and a CP-odd (A) Higgs bosons through the experimental signature of the process $pp \to H \to ZA \to l^+l^-b\bar{b}$. The theoretical context is a two-Higgs-doublet-model with twisted custodial symmetry, leading to a mass triplet $m_{H^\pm} \sim m_H$, and low-mass pseudoscalar A. The hypothesis of Type II Yukawa couplings is considered. The search exploits an integrated luminosity of 2.3 fb^{-1} collected in 2015 by the CMS experiment at 13 TeV center-of-mass energy.

1 Introduction

The simultaneous discovery by ATLAS and CMS of a neutral boson with a mass close to 125 GeV during the first LHC run [1, 2] not only motivates the measurement of its properties, but also the studies of the related scalar sector nature. Extensions of the scalar sector of the standard model (SM) predict the existence of additional Higgs bosons. A simple scenario is the two Higgs doublet model (2HDM), where a second doublet of complex scalar fields is added to the minimal SM scalar sector lagrangian. The generic 2HDM potential [3] has a large number of degrees of freedom. Assuming the preservation of the electromagnetic gauge symmetry, the CP invariance on the bosonic sector of the theory, the choice of the custodial phase and the suppression of the tree-level flavour-changing neutral currents, the number of free parameters is reduced to six. If the twisted custodial symmetry is considered, the free parameters of the theory are the mass of the Higgs bosons h (m_h), the mass of the pseudoscalar A (m_A), the triplet mass m_T defined by the masses of the charged Higgs bosons ($m_{H^\pm}$) and the CP-even state H (m_H), the ratio of the vacuum expectation values $\tan\beta$, and the mixing angle α between the two CP-even eigenstates. In the non-twisted custodial symmetry scenario, e.g. characteristic of the MSSM scalar sector, A and H are exchanged, leading to a mass triplet $m_T : m_{H^\pm} \sim m_A$.

Several Higgs boson mass hierarchies are possible. The *MSSM*-like hierarchy implies a heavy pseudoscalar while other studies [3–5] have shown that an inverted mass hierarchy (im2HDM) with a heavy H and a light pseudoscalar is possible and well motivated. This is illustrated in Fig 1 (left).

This work follows the previous search on a similar topic [6], where a pseudoscalar and a Z/γ^* boson (henceforth simply denoted Z boson) are decay products of a heavier H boson. This situation is described in the context of the twisted custodial symmetry. An example of the branching fractions of H and A, calculated with 2HDMC [7] for m_H = 300 GeV and m_A = 200 GeV, is shown in Fig 1 (right). The branching fractions show a large dependency on $\beta - \alpha$, and in the limit where $\cos(\beta - \alpha)$ is close to zero, the decay of the heavier neutral boson to a Z and a lighter boson is among the largest.

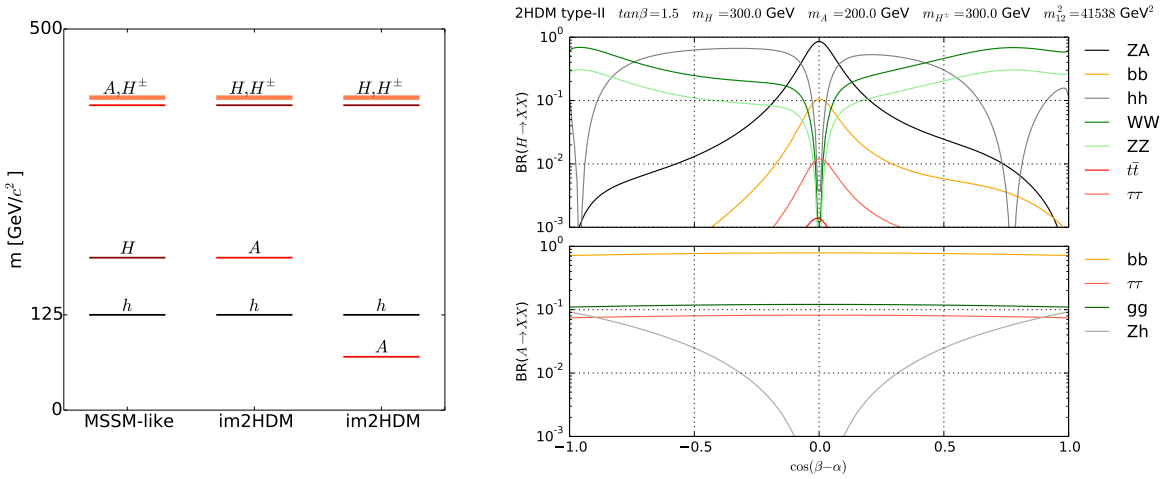

Figure 1: Left: 2HDM hierarchies considered in this search. Right: Branching fractions of the H and A bosons, for $\tan\beta = 1.5$, m_H = 300 GeV, $m_A = 200$ GeV and $m_{12}^2 = 41538$ GeV^2.

In the 2HDM, the dependency of the neutral boson couplings to the gauge bosons is given by:

$$\frac{g_{hVV}}{g_{hVV}^{SM}} = \sin(\beta-\alpha), \frac{g_{HVV}}{g_{hVV}^{SM}} = \cos(\beta-\alpha). \quad (1)$$

In the limit $\cos(\beta-\alpha)=0$, the boson h behaves exactly as the SM higgs boson, and the heavy H is decoupled from the gauge bosons. This *alignment limit* scenario is favoured by the measurement of the couplings of the 125 GeV boson [8]. The branching fractions of the H and A bosons are shown in Fig. 2 (left) for $\cos(\beta-\alpha)=0.01$, $m_A = 200$ GeV and $m_H = 300$ GeV, with respect to the value of $\tan\beta$. In the $\tan\beta$ range between 0.5 and 1.5 [8], the decay mode $H \to ZA$ is largely dominant. The decay mode $A \to b\bar{b}$ is significant above $\tan\beta \sim 0.5$ (and dominates above $\tan\beta \sim 1$), i.e. where the coupling to the top quarks becomes sufficiently small. In the context where $\cos(\beta-\alpha) \sim 0$ and $0.5 < \tan\beta < 1.5$, the decay modes $H \to ZA$ and $A \to b\bar{b}$ are particularly interesting experimentally, and therefore define the final state considered in this work.

The decay of the Z boson into a pair of muons or a pair of electrons, together with the dominant decay of the A boson into a pair of b quarks, leads to the final state composed of a pair of same-flavour and opposite-sign leptons in association with a pair of b jets. The equivalent Next-to-Next-to-Leading-Order (NNLO) cross section evaluated with SusHI [9] and 2HDMC for different values of m_A and m_H is shown in Fig. 2 (right). It assumes the soft $\mathbb{Z}_2$-breaking mass to be $m_{12}^2 = m_{H^\pm}^2 \frac{\tan\beta}{1+\tan\beta^2}$, $\tan\beta = 1.5$, $m_t = 173.2$ GeV and $\alpha_s(m_Z) = 0.117$. The cross section reaches at most 500 fb for the lowest values of m_A, and m_H typically below 500 GeV. It drops quickly as either the mass of the A or H boson increases. The increase of cross section observed around $m_H \sim 350$ GeV corresponds to the range where the top quarks involved in the $gg \to H$ coupling (through the top-quark loop) become on-shell.

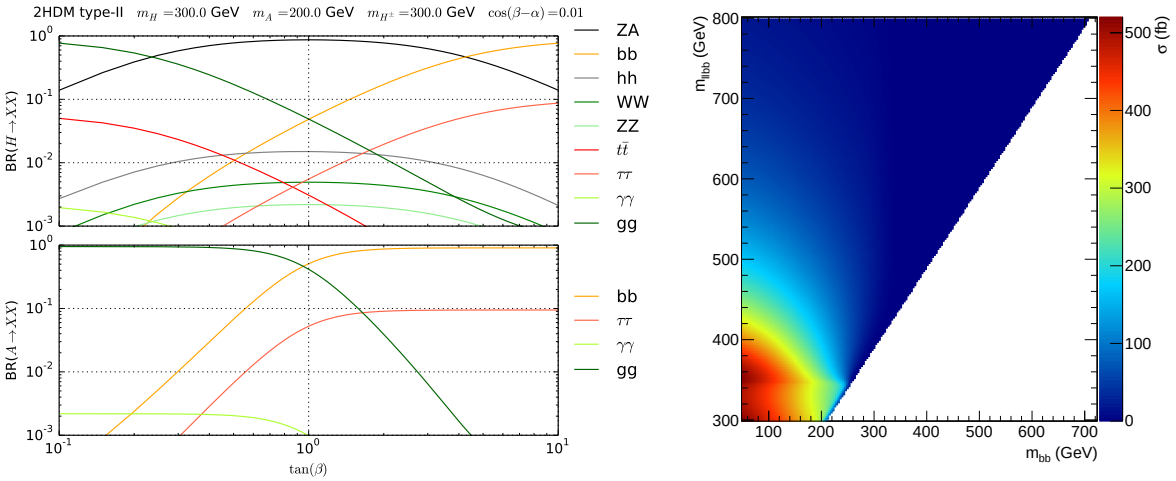

Figure 2: Left: Branching fractions of the H and A, for $\cos(\beta-\alpha) = 0.01$, m_H = 300 GeV, $m_A = 200$ GeV. Right: Cross section of $pp \to H \to ZA \to llb\bar{b}$ (in fb).

Several SM processes with a production cross section relatively large compared to that of the signal yield the final state. The background process with the largest cross section is the Drell-Yan (DY) $pp \to Z$+jets. First, there are $pp \to Z$+jets events with jets from initial-state radiation initiated by the emission of b quarks, and second, light and c jets have a non negligible probability to be tagged as originating from a b quark, and therefore mimick the signal signature. The other dominant background process is the production of top-antitop quark pairs ($t\bar{t}$), each

decaying into a W boson and a b quark. Finally, background processes with a smaller cross section are also considered: single-top, ZZ and Zh.

In this work, the background level is controlled in a partly data-driven manner as described below by measuring the background in a control region, and extrapolating it in the signal region using the simulated prediction. This follows to some extent the approach adopted in [6] and fits the needs given the available statistics from the 2015 Run II data taking.

Thirteen signal hypotheses are defined from particular choices of m_A and m_H. The Higgs bosons mass choices (henceforth denoted $\mathcal{H}_A^H$ with H and A in GeV) are $\mathcal{H}_{50}^{300}$, $\mathcal{H}_{100}^{300}$, $\mathcal{H}_{200}^{300}$, then $\mathcal{H}_{50}^{500}$, $\mathcal{H}_{100}^{500}$, $\mathcal{H}_{200}^{500}$, $\mathcal{H}_{300}^{500}$, $\mathcal{H}_{400}^{500}$, and finally $\mathcal{H}_{50}^{800}$, $\mathcal{H}_{100}^{800}$, $\mathcal{H}_{200}^{800}$, $\mathcal{H}_{400}^{800}$ and $\mathcal{H}_{700}^{800}$.

For each $\mathcal{H}_A^H$, a signal region $\mathcal{S}_A^H$ is defined in the plane formed by m_{bb} and m_{llbb} (henceforth denoted $\mathcal{P}$) as a rectangle centered on $\mathcal{H}_A^H$. The size of $\mathcal{S}_A^H$ is set to three times the experimental resolution. At small Higgs boson masses, the experimental width of the signal is driven by the detector resolution, while for higher masses (or large mass gap between m_A and m_H), the natural width may be dominant. The experimental resolution is typically 15% of the Higgs boson masses. In addition, each $\mathcal{S}_A^H$ is also defined by a restriction on the invariant mass of the two opposite charge and same flavour leptons, which has to be between 75 and 105 GeV, in order to reduce the $\bar{t}t$ contamination.

Correspondingly, control regions $\mathcal{C}_A^H = \mathcal{P} - \mathcal{S}_A^H$ are used to control the background level normalization. The condition that invariant mass of the two opposite-charge and same-flavour leptons is between 60 and 120 GeV is applied as an additional constraint on all $\mathcal{C}_A^H$. The estimation of the background normalization is done by fitting the m_{ll} distribution in $\mathcal{C}_A^H$.

The evaluation of the background contamination in each $\mathcal{S}_A^H$ using the comparison of data and the prediction from theory in $\mathcal{C}_A^H$ allows to establish the upper limit on the cross section of $pp \to H \to ZA \to l^+l^-b\bar{b}$ for each $\mathcal{H}_A^H$.

Section 2 of this note describes the experimental apparatus and the set of simulated event samples used in this work. Section 3 describes the event reconstruction and selection, Sec. 4 details the background control and lists the systematic uncertainties, and finally the results and the conclusions are found in Sec. 5 and Sec. 6 .

2 CMS detector and simulated samples

The central feature of the CMS apparatus is a superconducting solenoid of 6 m internal diameter, providing a magnetic field of 3.8 T. Within the superconducting solenoid volume are a silicon pixel and strip tracker, a lead tungstate crystal electromagnetic calorimeter (ECAL), and a brass and scintillator hadron calorimeter (HCAL), each composed of a barrel and two endcap sections. Forward calorimeters extend the pseudorapidity (η) [10] coverage provided by the barrel and endcap detectors. Muons are measured in gas-ionization detectors embedded in the steel flux-return yoke outside the solenoid. The first level (L1) of the CMS trigger system, composed of custom hardware processors, uses information from the calorimeters and muon detectors to select the most interesting events in a fixed time interval of less than 4 μs. The high-level trigger (HLT) processor farm further decreases the event rate from around 100 kHz to less than 1 kHz, before data storage.

A more detailed description of the CMS detector, together with a definition of the coordinate system used and the relevant kinematic variables, can be found in Ref. [10].

The samples of the signal events for different m_A and m_H, as well the samples of background

events, are modeled using various event generators, and can be compared with the recorded data thanks to the CMS response simulation based on GEANT 4.

The thirteen signal samples, each corresponding to one $\mathcal{H}_A^H$, are produced at tree-level using MADGRAPH_aMC@NLO 5.2.2.3 [11] interfaced with the parton shower (PS) generator PYTHIA 8.2 [12]. The parton distribution function (PDF) is NNPDF 2.3 lo 4F [13], and the factorization and renormalization scales are estimated dynamically. The shower tune is the CUEPT8M1, derived from the MONASH tune [14]. Only one partonic multiplicity is considered in the ME calculation, hence no ME+PS merging technique is needed. The justification of this choice is that the uncertainties on initial-state radiation modeling is expected to be negligible in the context of this study. The value of $\tan\beta$ is set to 1.5, and that of $\cos(\beta-\alpha)$ to 0.01, and the width of each Higgs boson is predicted by the matrix-element calculation. As an illustration, the width of the H boson is, for $\tan\beta = 1.5$: $\Gamma_H \sim 6$ GeV for $\mathcal{H}_{50}^{300}$, $\Gamma_H \sim 230$ GeV for $\mathcal{H}_{50}^{800}$ and $\Gamma_H \sim 15$ GeV for $\mathcal{H}_{700}^{800}$. The cross section of each signal sample [15] is the product of the NNLO cross section for the process pp $\rightarrow$ H calculated with SusHI and the branching fractions estimated with 2HDMC.

There are two dominant background processes to be considered. First, the production of a Z boson in association with a pair of b quarks. This process has been studied at Tevatron and with the LHC Run I data by both CMS and ATLAS, and is shown to be correctly described by the most recent simulation tools if the two b jets are sufficiently hard and well separated [16–18]. This process is modeled using MADGRAPH_aMC@NLO 5.2.2.3 interfaced with PYTHIA 8.2, using the matrix-element (ME) calculation of $pp \rightarrow l^+l^- + 0,1,2$ partons at Next-to-Leading-Order (NLO) in QCD. The merging of the ME+PS description is done with the FxFx scheme [19], based on a merging scale of 30 GeV. The PDF used is NNPDF 3.0 nlo. The normalization is set to the NNLO production cross section in QCD [20].

The second dominant background process in this study is the production of a pair of top quarks, each providing naturally a b jet and either jets or a lepton and missing transverse energy. The $\mathrm{t\bar{t}}$ background is simulated with POWHEG v.2 interfaced with PYTHIA 8.2. The PDF in that case is NNPDF 3.0 nlo (with $\alpha_s(M_Z) = 0.118$). The normalization is set to the NNLO (+NNLL) production cross section in QCD [21].

Other background processes with a smaller impact in this study are present as well. The s- and t-channels of the single top production is modeled with MADGRAPH_aMC@NLO 5.2.2.3 interfaced with PYTHIA 8.2, in the 4-flavour numbering scheme, i.e. not including the b quarks as initial states of the involved Feynman diagrams. The PDF used is NNPDF 3.0 nlo. The production cross section of both channels is estimated at the NLO precision in QCD [22, 23]. The associated tW process is modeled using POWHEG v.2 interfaced with PYTHIA 8.2 in the 5-flavour numbering scheme. The PDF in that case is NNPDF 3.0 nlo, the production cross section is estimated at NNLO in QCD [24, 25]. The diboson process involving two Z bosons, one decaying into a pair of leptons, and the other decaying into a pair of quarks is modeled at NLO with MADGRAPH_aMC@NLO 5.2.2.3 interfaced with PYTHIA 8.2, with up to one parton in the ME calculation. The PDF in that case is NNPDF 3.0 nlo. The production cross section is evaluated at the NLO in QCD. The production of the 125 GeV h boson through the Higgstrahlung process Zh, with h$\rightarrow \mathrm{b\bar{b}}$ is also considered as a background. The modeling is this process is carried out using POWHEG v.2 interfaced with PYTHIA 8.2 with NNPDF 3.0 nlo as PDF. The production cross section is calculated including NNLO QCD and NLO EW corrections [26].

Additional piled-up interactions (PU) per bunch crossing are included in the simulation to match the PU distribution observed in data.

3 Event reconstruction and selection

The first step of this search is the online selection of the events based on the dilepton triggers. The study is based on the 2015 Run D dataset, totalizing 2.3 fb^{-1} of integrated luminosity. Besides loose identification and isolation criteria, the lepton candidates are required to have a sufficiently large transverse momentum (p_T). In both the muon and electron cases, the thresholds are asymmetric: 17 and 8 GeV for the first case, 17 and 12 GeV for the second case.

The final selection of electrons [27] and muons [28] relies on the particle-flow (PF) [29, 30] event algorithm output. The PF algorithm reconstructs and identifies each individual particle with an optimized combination of information from the various elements of the CMS detector. The energy of electrons is determined from a combination of the electron momentum at the primary interaction vertex as determined by the tracker, the energy of the corresponding ECAL cluster, and the energy sum of all bremsstrahlung photons spatially compatible with originating from the electron track. The transverse momentum of muons is obtained from the curvature of the corresponding track.

Both electrons and muons are required to have at least 20 GeV of p_T and be within the η range $|\eta| < 2.4$. The origin of the leptons must be compatible with the primary pp interaction (identified as the vertex with the largest quadratic sum of its constituent tracks p_T). This is done by imposing that the distance of closest approach between the vertex and the lepton track is less than or equal to five times the sum of the vertex and track position resolution. Both leptons must fulfill an isolation condition, computed using the PF technique. The isolation of the muon (electron) is defined as the ratio (R) between the scalar sum of p_T or energy of PF objects in a cone of 0.4 (0.3) around the muon (electron), divided by the p_T of the lepton. The isolation is corrected for the contamination from PU interactions occurring at each bunch crossing. R must be at most 0.25 for the muons, while for the electrons it is at most 0.035 in the barrel region ($|\eta| < 1.479$), and 0.064 in the endcap region ($1.479 < |\eta| < 2.4$). The lepton reconstruction and identification efficiency differences observed between the data and the simulation require defining a correction factor (C_l) to be applied on the simulation to compensate for these differences as a function of the lepton p_T and η.

The distribution of the invariant mass of the two leptons (m_{ll}) is shown in Fig. 3. The dimuon case (left) shows an excellent agreement between data and prediction from theory. The small discrepancy observed between 80 and 95 GeV in Fig. 3 (right) comes from a slight misestimation of the electron energy scale .

Jet momentum is determined as the vectorial sum of all PF particle momenta in the jet, built with the anti-k_T algorithm [31, 32], using a jet radius of 0.4. Only jets with at least $p_T > 30$ GeV and $\eta < 2.4$ are retained for the analysis. The reconstructed jet momentum is found from simulation to be within 5% to 10% of the true momentum over the whole p_T spectrum and detector acceptance. An offset correction is applied to jet energies to take into account the contribution from additional proton-proton interactions within the same bunch crossing. Jet energy corrections are derived from simulation and are confirmed with in situ measurements of the energy balance in dijet and photon+jet events. Additional selection criteria are applied to each event to remove spurious jet-like features originating from isolated noise patterns in certain HCAL regions. Jets quality criteria require less than 90% of the neutral electromagnetic (EM) and hadronic deposits to come from neutral particles and that the jet be composed of two or more objects. Additionally, tight jets are required to have a charged hadron fraction and multiplicity greater than zero as well as a charged EM fraction smaller than 99%.

The b tagging of the reconstructed jets is realized through the use of the new version of the

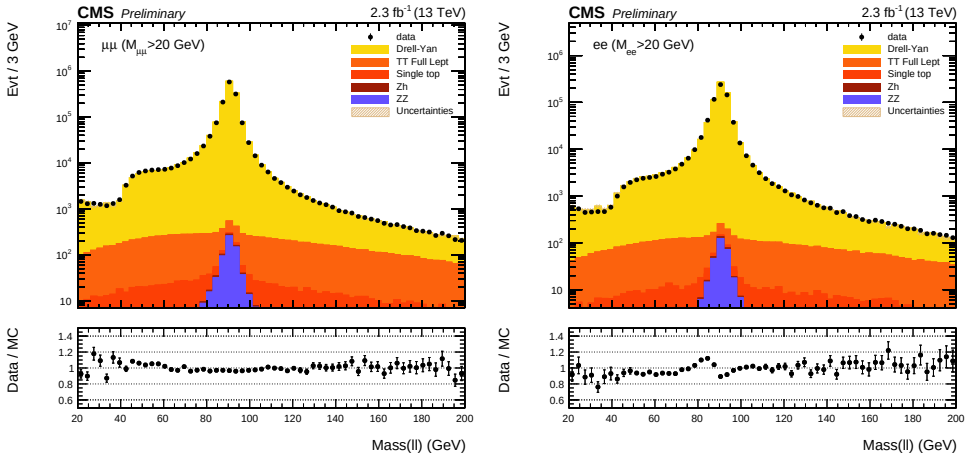

Figure 3: Left: invariant mass distribution for the dimuon system. Right: same for the electrons. The brown shaded band is the MC statistical uncertainty, and the error bars is the data statistical uncertainty.

Combined Secondary Vertex (CSV) algorithm, prepared for the Run II, which combines in one output the long lifetime and heavy-flavour characteristics of the b hadrons. It is an MLP-based discriminator, which uses among others the secondary vertex mass, the multiplicity of charged particles associated to the secondary vertex, the flight significance associated to the secondary vertex and the energy of charged particles associated to the secondary vertex divided by the energy of all charged particles associated to the jet. The b tagging efficiency difference observed between the data and the simulation requires defining a correction factor (C_b) to be applied on the simulation to compensate these differences, as a function of the jet p_T, η and flavour. The discriminant distribution (output of the CSV algorithm) obtained from the two leading jets in the dilepton events with at least two jets is shown in Fig. 4, prior to C_b application. In this analysis, jets are tagged as originating from a b quark if the CSV discriminant is higher than 0.8.

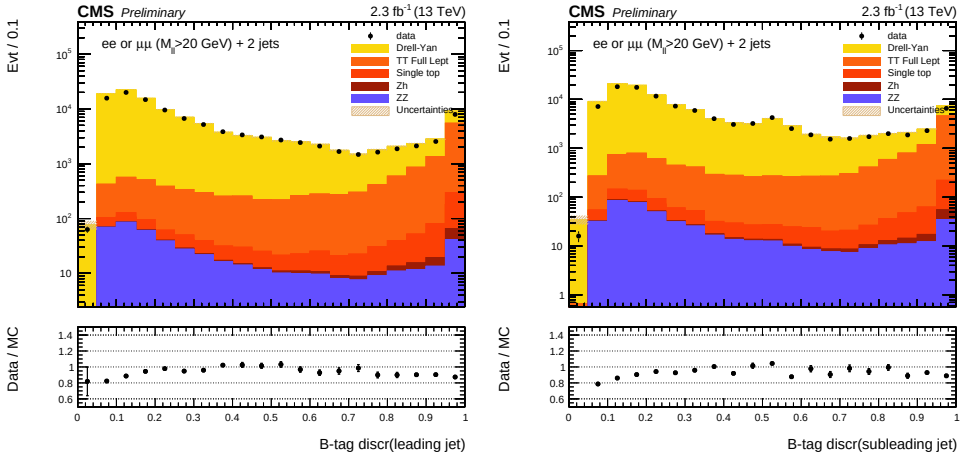

Figure 4: B-tagging discriminant for the leading jet (left) and subleading jet (right) in p_T, for Z+>=2 jets. The brown shaded band is the MC statistical uncertainty, and the error bars are the data statistical uncertainty. No C_b is applied on the simulation to match the data.

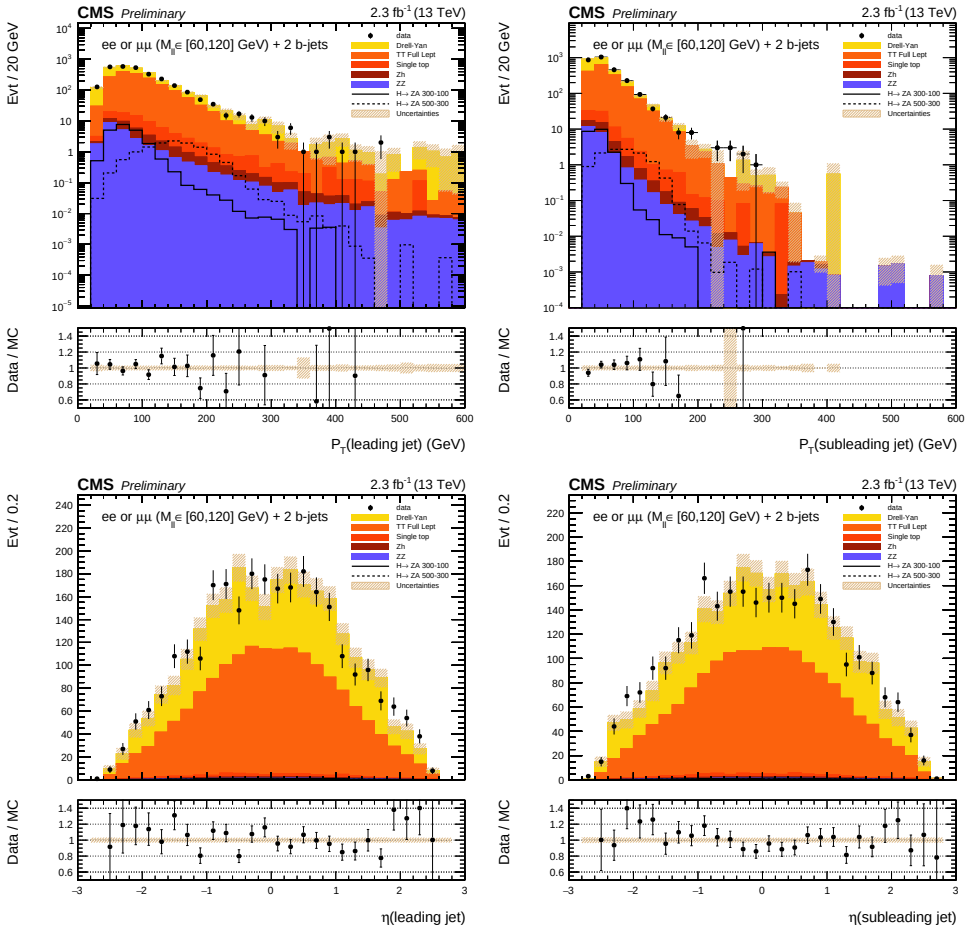

Figure 5: From left to right, and top to bottom: p_T of the leading jet; p_T of the sub-leading jet, η of the leading jet; η of the sub-leading jet. The brown shaded band is the MC statistical uncertainty, and the error bars is the data statistical uncertainty. The distributions are obtained after the fit on the background.

4 Background control and systematic uncertainties

As discussed in Sec. 1, the signature of the events of interest for this work is defined by the presence of two opposite-charge and same-flavour leptons, as well as two jets tagged as originating from a b quark. For each $\mathcal{H}_A^H$, a fit is performed in $\mathcal{C}_A^H$ to match the background processes to the data. The fit is performed using the invariant mass of the dilepton system, which allows the distinction between the DY (dominated by the associated production of a Z boson and a pair of b quarks) and the $t\bar{t}$ components.

The rescaling factor obtained from the fit, together with the resulting statistical and systematic uncertainties, are propagated into $\mathcal{S}_A^H$, and the comparison between the data and the predicted background processes is used for a statistical interpretation either in terms of agreement between the data with the SM prediction, or with a particular signal hypothesis. Typically, the scaling factor for the DY process is close to -20%, while the one for the $t\bar{t}$ is -5%, and it remains stable from one $\mathcal{C}_A^H$ choice to another. The p_T of the two leading jets ordered in p_T and their η distribution, after fitting the predictions from theory to the data in one of the control regions, are shown in Fig. 5.

Different sources of systematic uncertainties are considered in the background fitting proce-

dure:

- The uncertainty on the jet energy corrections (JEC) and resolution, which aligns the measured and the generated jet momentum. The JEC uncertainties are evaluated by applying a 1-σ deviation with respect to the default correction factors.
- The uncertainty on the b tagging of the jets is obtained by varying C_b on the predictions from theory by one standard deviation (up and down). The b-tagging scale factor variation is taken to be correlated with the c-mistag scale factor variation, while the light scale factor variation are considered uncorrelated.
- The uncertainty on PU is obtained by varying the hypothesis on the minimum bias cross section by 5%.
- The uncertainty on the luminosity (2.7%).
- The uncertainty on the lepton reconstruction and identification efficiency is obtained by varying C_l by one standard deviation. Typically, this leads to a 2% effect on the event acceptance.
- The uncertainties on the predictions from theory for the dominant backgrounds are obtained as follows. The shape uncertainty on the factorization and renormalization scales is obtained by varying them by a factor two, independently, excluding the variations $\{\mu_F, \mu_R\}$: $\{\times 2, /2\}$ and $\{/2, \times 2\}$ [33, 34]. The shape uncertainty on the PDF is estimated in the same way, running on the PDF replicas of the NNPDF 3.0 PDF set. For both cases, an envelope is computed, and the respective upper and lower limits represent the shape uncertainties for the predictions from theory. The uncertainty on the normalization is directly deduced from the uncertainties of the cross sections described in Section 2, and impacts the background fit independently from the PDF and scale shape uncertainties.

The comparison between data and the prediction from theory for the distribution of m_{bb} and m_{llbb} are shown in Fig. 6, together with the uncertainty band resulting from the quadratic sum of the systematic uncertainties discussed above. In addition, the predictions for the signal shape for $\mathcal{H}^{500}_{300}$ and $\mathcal{H}^{300}_{100}$ are shown in overlay.

5 Results

This work aims at finding new resonances in the l^+l^- + 2 b jets final state, which may correspond to a 2HDM Type II signature from the process pp $\rightarrow$ H $\rightarrow$ ZA. This search is done for three choices of m_H and for each of them, between three and five hypotheses of m_A are considered. For each $\mathcal{S}^H_A$ definition, corresponding to one $\mathcal{H}^H_A$ hypothesis, the upper limits are computed on the basis of two histograms. First, the m_{ll} distribution in $\mathcal{C}^H_A$, and second, the 1-bin content in $\mathcal{S}^H_A$. The dielectron and dimuon contributions are summed. The calculation of the limits done on that basis is used to derive model-independent limits on the cross section of a new signal. These limits are valid for models in which the width does not impact the efficiency and acceptance of the signal in $\mathcal{S}^H_A$ compared to that of the simulated samples used to derive the model-independent limits. This means that the Higgs bosons widths must be either small compared to the typical 15% resolution on the Higgs boson masses, or smaller than the widths corresponding to the generated samples used to compute the limits (width criterion).

The expected and observed limits are shown for each $\mathcal{H}^H_A$ in Fig. 7. The green and yellow shaded bands represent the 1- and 2-σ uncertainty bands. For $m_H = 300$ GeV, the expected limit on $\sigma \times BR$ ranges from $\sim$ 200 fb to $\sim$ 1 pb. For $m_H = 500$ GeV, the expected limit is

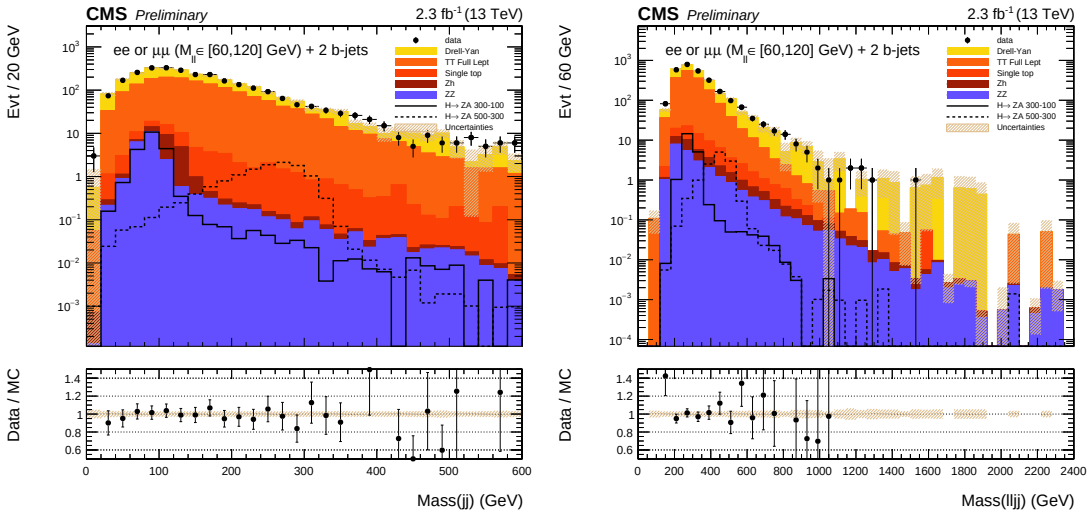

Figure 6: The distribution of the m_{bb} (left) and m_{llbb} (right). The shaded bands show the quadratic sum of the systematic uncertainties, and the error bars show the data and MC statistical uncertainties added quadratically. The predictions for the signal shape for $\mathcal{H}^{500}_{300}$ and $\mathcal{H}^{300}_{100}$ are shown in overlay.

generally lower, from around 80 fb for the lowest m_A hypothesis, up to reaches $\sim$ 250 fb for large m_A. The situation is similar for $m_H = 800$ GeV. An interesting aspect is that for $\mathcal{H}^{800}_{50}$ the sensitivity degrades due to the increasing collinearity of the two jets tagged as originating from a b quark. The observed limits, for each $\mathcal{H}^{H}_{A}$, are in agreement with the expected limits. The CLs criterion [35, 36], used to determine at 95% confidence level (CL) the upper limits on the signal cross section, are derived with the asymptotic method reported in [37].

In comparison to the results from the similar studies done with the data accumulated during the first LHC Run [6], the model-independent limits are not as stringent in this case. The reason for this is a trade-off between the change of the parton (essentially gluon) luminosity with the increase of the center-of-mass energy at Run II, and a ratio close to one order of magnitude between the respective integrated luminosities in Run I and Run II.

The predicted cross section of $pp \to H \to ZA \to l^+l^-b\bar{b}$ is also shown, for $\tan\beta = 0.5$, 1 and 1.5 (for $m_H = 300$ GeV), $\tan\beta = 1$ and 1.5 (for $m_H = 500$, 800 GeV). The predictions for $\tan\beta = 0.5$ are not shown for $\mathcal{H}^{800/500}_{x}$ because they do not fulfill the width criterion discussed previously. The uncertainty band is obtained by adding quadratically the PDF and scale uncertainties. The PDF uncertainty is estimated by comparing the cross sections obtained with CT10 [38], NNPDF 3.0 and MMHT [39]. The scale uncertainty is deduced by varying the factorization and normalization scales by a factor 2, independently. It turns out that over the entire set of tested masses, three points can already be excluded so far. These are $\mathcal{H}^{300}_{50}$ for $\tan\beta$ =1 and 0.5, $\mathcal{H}^{500}_{50}$ for $\tan\beta$ =1 and 1.5, and $\mathcal{H}^{500}_{100}$ for $\tan\beta$ =1.

6 Conclusion

This note describes the search for the signature of the process $pp \to H \to ZA \to l^+l^-b\bar{b}$, using the Run II data recorded by the CMS detector in 2015, for a total integrated luminosity of 2.3 fb^{-1}. The experimental final state is composed of a pair of opposite-charge and same-flavour leptons with m_{ll} between 75 and 105 GeV, and two jets tagged as originating from a b

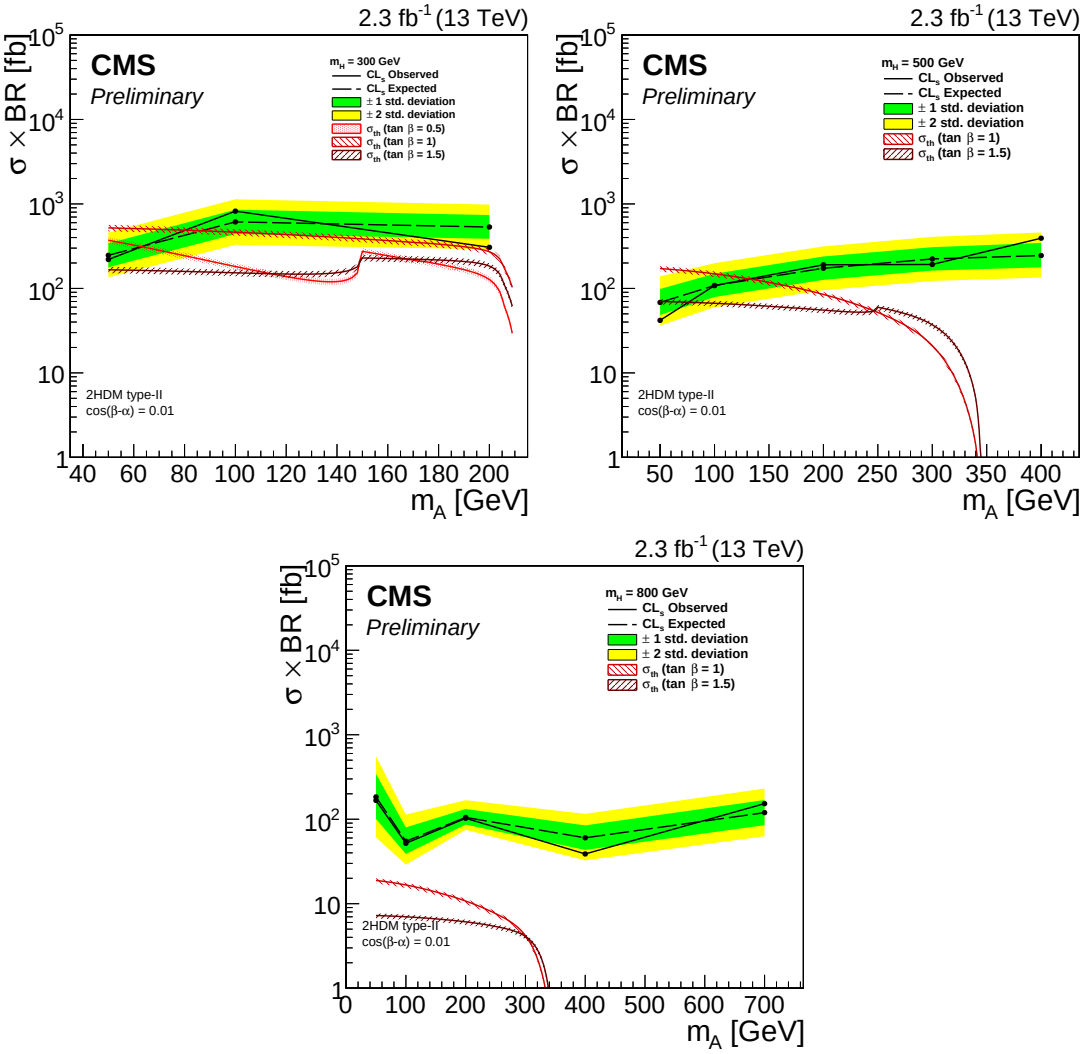

Figure 7: Limit on the $\sigma \times \mathrm{BR}(\mathrm{H} \to \mathrm{ZA}) \times \mathrm{BR}(\mathrm{Z} \to \mathrm{ll}) \times \mathrm{BR}(\mathrm{A} \to \mathrm{b\bar{b}})$, for $\mathrm{m_H}$ = 300, 500, 800 GeV. The predicted production cross section of $\mathrm{pp} \to \mathrm{H} \to \mathrm{ZA} \to \mathrm{l^+l^-b\bar{b}}$ are also shown for different values of tan β.

quark. For a series of m_A and m_H hypotheses, a rectangular signal region and a complementary control region are defined in the plane formed by m_{bb} and m_{llbb}. The search is performed by counting events in each signal region. For each mass hypothesis, the normalization of the standard model background processes is done on data in the control region, and propagated into the signal region. At this stage, no significant deviations from the standard model expectation are observed for $m_H = 300$, 500 and 800 GeV.

Model-dependent interpretations are also presented in the context of the Type-II 2HDM, with $\cos(\beta - \alpha) = 0.01$. In this context, the mass hypothesis corresponding to m_H = 300 GeV and m_A = 50 GeV is excluded for $\tan\beta = 1$ and 0.5. The mass hypothesis m_H = 500 GeV, m_A = 50 GeV is excluded for $\tan\beta$ =1 and 1.5. Finally the mass hypothesis m_H = 500 GeV, m_A = 100 GeV is also excluded for $\tan\beta$ =1.

References

[1] ATLAS Collaboration, "Observation of a new particle in the search for the Standard Model Higgs boson with the ATLAS detector at the LHC", *Phys.Lett.* **B716** (2012) 1–29, doi:10.1016/j.physletb.2012.08.020, arXiv:1207.7214.

[2] CMS Collaboration, "Observation of a new boson at a mass of 125 GeV with the CMS experiment at the LHC", *Phys.Lett.* **B716** (2012) 30–61, doi:10.1016/j.physletb.2012.08.021, arXiv:1207.7235.

[3] G. C. Branco et al., "Theory and phenomenology of two-Higgs-doublet models", *Phys. Rept.* **516** (2012) 1–102, doi:10.1016/j.physrep.2012.02.002, arXiv:1106.0034.

[4] J. M. Gerard and M. Herquet, "A Twisted custodial symmetry in the two-Higgs-doublet model", *Phys. Rev. Lett.* **98** (2007) 251802, doi:10.1103/PhysRevLett.98.251802, arXiv:hep-ph/0703051.

[5] S. de Visscher et al., "Unconventional phenomenology of a minimal two-Higgs-doublet model", *JHEP* **0908** (2009) 042, doi:10.1088/1126-6708/2009/08/042, arXiv:0904.0705.

[6] CMS Collaboration, "Search for neutral resonances decaying into a Z boson and a pair of b jets or tau leptons", arXiv:1603.02991.

[7] D. Eriksson, J. Rathsman, and O. Stal, "2HDMC: Two-Higgs-Doublet Model Calculator Physics and Manual", *Comput. Phys. Commun.* **181** (2010) 189–205, doi:10.1016/j.cpc.2009.09.011, arXiv:0902.0851.

[8] ATLAS Collaboration, "Constraints on new phenomena via Higgs boson couplings and invisible decays with the ATLAS detector", *JHEP* **11** (2015) 206, doi:10.1007/JHEP11(2015)206, arXiv:1509.00672.

[9] R. V. Harlander, S. Liebler, and H. Mantler, "SusHi: A program for the calculation of Higgs production in gluon fusion and bottom-quark annihilation in the Standard Model and the MSSM", *Comput. Phys. Commun.* **184** (2013) 1605–1617, doi:10.1016/j.cpc.2013.02.006, arXiv:1212.3249.

[10] CMS Collaboration, "The CMS experiment at the CERN LHC", *JINST* **3** (2008) S08004, doi:10.1088/1748-0221/3/08/S08004.

[11] J. Alwall et al., "The automated computation of tree-level and next-to-leading order differential cross sections, and their matching to parton shower simulations", *JHEP* **1407** (2014) 079, doi:10.1007/JHEP07(2014)079, arXiv:1405.0301.

[12] T. Sjostrand et al., "An Introduction to PYTHIA 8.2", *Comput. Phys. Commun.* **191** (2015) 159–177, doi:10.1016/j.cpc.2015.01.024, arXiv:1410.3012.

[13] NNPDF Collaboration, "Parton distributions for the LHC Run II", *JHEP* **04** (2015) 040, doi:10.1007/JHEP04(2015)040, arXiv:1410.8849.

[14] P. Skands, S. Carrazza, and J. Rojo, "Tuning PYTHIA 8.1: the Monash 2013 Tune", *Eur. Phys. J.* **C74** (2014), no. 8, 3024, doi:10.1140/epjc/s10052-014-3024-y, arXiv:1404.5630.

[15] R. Harlander et al., "Interim recommendations for the evaluation of Higgs production cross sections and branching ratios at the LHC in the Two-Higgs-Doublet Model", arXiv:1312.5571.

[16] ATLAS Collaboration, "Measurement of differential production cross-sections for a Z boson in association with b-jets in 7 TeV proton-proton collisions with the ATLAS detector", *JHEP* **10** (2014) 141, doi:10.1007/JHEP10(2014)141, arXiv:1407.3643.

[17] CMS Collaboration, "Measurement of the production cross sections for a Z boson and one or more b jets in pp collisions at sqrt(s) = 7 TeV", *JHEP* **1406** (2014) 120, doi:10.1007/JHEP06(2014)120, arXiv:1402.1521.

[18] CMS Collaboration, "Measurement of the cross section and angular correlations for associated production of a Z boson with b hadrons in pp collisions at $\sqrt{s} = 7$ TeV", *JHEP* **1312** (2013) 039, doi:10.1007/JHEP12(2013)039, arXiv:1310.1349.

[19] R. Frederix and S. Frixione, "Merging meets matching in MC@NLO", *JHEP* **1212** (2012) 061, doi:10.1007/JHEP12(2012)061, arXiv:1209.6215.

[20] R. Gavin, Y. Li, F. Petriello, and S. Quackenbush, "FEWZ 2.0: A code for hadronic Z production at next-to-next-to-leading order", *Comput. Phys. Commun.* **182** (2011) 2388–2403, doi:10.1016/j.cpc.2011.06.008, arXiv:1011.3540.

[21] M. Czakon and A. Mitov, "Top++: A Program for the Calculation of the Top-Pair Cross-Section at Hadron Colliders", *Comput. Phys. Commun.* **185** (2014) 2930, doi:10.1016/j.cpc.2014.06.021, arXiv:1112.5675.

[22] P. Kant et al., "HatHor for single top-quark production: Updated predictions and uncertainty estimates for single top-quark production in hadronic collisions", *Comput. Phys. Commun.* **191** (2015) 74–89, doi:10.1016/j.cpc.2015.02.001, arXiv:1406.4403.

[23] M. Aliev et al., "HATHOR: HAdronic Top and Heavy quarks crOss section calculatoR", *Comput. Phys. Commun.* **182** (2011) 1034–1046, doi:10.1016/j.cpc.2010.12.040, arXiv:1007.1327.

[24] N. Kidonakis, "Two-loop soft anomalous dimensions for single top quark associated production with a W- or H-", *Phys. Rev.* **D82** (2010) 054018, doi:10.1103/PhysRevD.82.054018, arXiv:1005.4451.

[25] N. Kidonakis, "Top Quark Production", in *Proceedings, Helmholtz International Summer School on Physics of Heavy Quarks and Hadrons (HQ 2013)*, pp. 139–168. 2014. arXiv:1311.0283. doi:10.3204/DESY-PROC-2013-03/Kidonakis.

[26] L. Altenkamp et al., "Gluon-induced Higgs-strahlung at next-to-leading order QCD", *JHEP* **02** (2013) 078, doi:10.1007/JHEP02(2013)078, arXiv:1211.5015.

[27] CMS Collaboration, "Performance of electron reconstruction and selection with the CMS detector in proton-proton collisions at $\sqrt{s} = 8$ TeV", *JINST* **10** (2015) P06005, doi:10.1088/1748-0221/10/06/P06005, arXiv:1502.02701.

[28] CMS Collaboration Collaboration, "Performance of CMS muon reconstruction in pp collision events at $\sqrt{s} = 7$ TeV", *JINST* **7** (2012) P10002, doi:10.1088/1748-0221/7/10/P10002, arXiv:1206.4071.

[29] CMS Collaboration, "Particle-flow event reconstruction in CMS and performance for jets, taus, and $E_{\mathrm{T}}^{\mathrm{miss}}$", CMS Physics Analysis Summary CMS-PAS-PFT-09-001, CERN, 2009.

[30] CMS Collaboration, "Commissioning of the particle-flow event with the first LHC collisions recorded in the CMS detector", CMS Physics Analysis Summary CMS-PAS-PFT-10-001, CERN, 2010.

[31] M. Cacciari, G. P. Salam, and G. Soyez, "The anti-k_t jet clustering algorithm", *JHEP* **04** (2008) 063, doi:10.1088/1126-6708/2008/04/063, arXiv:0802.1189.

[32] M. Cacciari, G. P. Salam, and G. Soyez, "FastJet user manual", *Eur. Phys. J. C* **72** (2012) 1896, doi:10.1140/epjc/s10052-012-1896-2, arXiv:1111.6097.

[33] M. Cacciari et al., "The t anti-t cross-section at 1.8-TeV and 1.96-TeV: A Study of the systematics due to parton densities and scale dependence", *JHEP* **04** (2004) 068, doi:10.1088/1126-6708/2004/04/068, arXiv:hep-ph/0303085.

[34] S. Catani, D. de Florian, M. Grazzini, and P. Nason, "Soft gluon resummation for Higgs boson production at hadron colliders", *JHEP* **07** (2003) 028, doi:10.1088/1126-6708/2003/07/028, arXiv:hep-ph/0306211.

[35] T. Junk, "Confidence level computation for combining searches with small statistics", *Nucl. Instrum. Meth.* **A434** (1999) 435–443, doi:10.1016/S0168-9002(99)00498-2, arXiv:hep-ex/9902006.

[36] A. L. Read, "Modified frequentist analysis of search results (The CL(s) method)", in *Workshop on confidence limits, CERN, Geneva, Switzerland, 17-18 Jan 2000: Proceedings*. 2000.

[37] G. Cowan, K. Cranmer, E. Gross, and O. Vitells, "Asymptotic formulae for likelihood-based tests of new physics", *Eur. Phys. J.* **C71** (2011) 1554, doi:10.1140/epjc/s10052-011-1554-0, 10.1140/epjc/s10052-013-2501-z, arXiv:1007.1727. [Erratum: Eur. Phys. J.C73,2501(2013)].

[38] M. Guzzi et al., "CT10 parton distributions and other developments in the global QCD analysis", arXiv:1101.0561.

[39] L. A. Harland-Lang, A. D. Martin, P. Motylinski, and R. S. Thorne, "Parton distributions in the LHC era: MMHT 2014 PDFs", *Eur. Phys. J.* **C75** (2015), no. 5, 204, doi:10.1140/epjc/s10052-015-3397-6, arXiv:1412.3989.